PHYSICAL REVIEW A **90**, 023630 (2014)

Miscible-immiscible quantum phase transition in coupled two-component Bose-Einstein condensates in one-dimensional optical lattices

Fei Zhan,[1,2] Jacopo Sabbatini,[1,2] Matthew J. Davis,[1] and Ian P. McCulloch[1,2]
[1]*School of Mathematics and Physics, The University of Queensland, St. Lucia, Queensland 4072, Australia*
[2]*Centre of Excellence for Engineered Quantum Systems, The University of Queensland, St. Lucia, Queensland 4072, Australia*
(Received 8 May 2014; published 26 August 2014)

We study the miscible-immiscible quantum phase transition in a linearly coupled binary Bose-Hubbard model in one dimension that can describe the low-energy properties of a two-component Bose-Einstein condensate in optical lattices. With the quantum many-body ground state obtained from the density matrix renormalization group algorithm, we calculate the characteristic physical quantities of the phase transition controlled by the linear coupling between the two components. Furthermore we calculate the Binder cumulant to determine the critical point and construct the phase diagram. The strong-coupling expansion shows that in the Mott insulator regime the model Hamiltonian can be mapped to a spin-1/2 *XXZ* model with a transverse magnetic field.

DOI: 10.1103/PhysRevA.90.023630 PACS number(s): 03.75.Nt, 64.70.Tg, 03.75.Mn, 05.10.Cc

I. INTRODUCTION

In recent years, the progress in single-atom detection and the manipulation of ultracold neutral atoms has allowed experimentalists to use these systems to engineer and emulate condensed matter systems [1,2]. Multicomponent Bose-Einstein condensates (BECs), formed by atoms of different atomic species or different hyperfine states, have attracted attention from both experimentalists [3,4] and theorists [5–7] due to their larger symmetry groups and extensive degrees of freedom. As the simplest model consisting of multiple components, the binary BEC has been an appealing candidate to simulate the spin-1/2 fermionic superconductor, magnetic behavior [8], superfluids [9], phase separation [10], quantum phase transitions [11,12], and thermalization [13].

Binary BECs are naturally divided into miscible and immiscible mixtures based on the interaction strengths characterizing the system. In a two-component BEC we can observe three kinds of interactions: interaction within the first component, interaction within the second component, and interaction between the two components. If the strength of the intercomponent interaction exceeds that of the intracomponent interactions, then energy considerations show that the two-components prefer to be in a phase-separated or immiscible state [10,14]. If the opposite is true then the system is said to be in the miscible phase.

A two-component BEC composed of bosons in different hyperfine states can, however, undergo a miscible-immiscible phase transition controlled by a linear coupling between the energy levels [15]. This phenomenon has been studied in a number of settings outside of optical lattices, such as nonlinear Josephson-type oscillations [16], nontopological vortices [17], and nonequilibrium dynamics across the critical point [18–20].

The dependence of the order parameter on the linear coupling coefficient revealed a second-order transition in a mean-field (MF) numerical study of this phase transition [15]. The properties of a second-order phase transition depend entirely on its universality class and are insensitive to the microscopic details of the underlying system. The universality class is determined by a set of power-law indices, called critical exponents, which characterize quantities such as the correlation length and the response time of the system [21]. Studies of the static properties of a system near the critical point are challenging because of the divergence of these quantities.

In this paper we study the miscible-immiscible phase transition of a linearly coupled two-component Bose-Hubbard model describing the low-energy physics of a binary BEC loaded in an optical lattice in one dimension. The numerical studies presented here explain future experiments for a two-component BEC in optical lattices and serve as a benchmark for studies of the nonequilibrium properties, for example, the verification of Kibble-Zurek theorem [11,12]. In addition, because now single-site resolved measurement in optical lattices is available in laboratories [2], the miscible-immiscible phase transition studied here should inspire qubit designs with two-component BECs in optical lattices [22].

The exponentially growing size of the Hilbert space as the lattice grows in size prevents the investigation of the full quantum state with exact diagonalization methods, even for lattices of moderate sizes. On the other hand, matrix product states (MPSs) can parametrize the size of the Hilbert subspace relevant to the low-energy properties by the dimension of the matrices, i.e., the number of states, and the size of the subspace grows polynomially with the lattice size [23]. In this paper we employ the MPS as the ansatz to represent the many-body state and the density matrix renormalization group (DMRG) to variationally solve for the ground state. Infinite DMRG (iDMRG) methods [24] exploiting the system's translational invariance in the thermodynamic limit allow us to compute the ground state of the system without boundary or finite-size effects. From the ground state we can determine a variety of observables like expectation values and multipoint correlations that help us characterize the quantum phase transition and its critical exponents. With the iDMRG methods the correlation length can be calculated directly from the eigenvalues of the transfer matrix.

The paper is organized as follows. In Sec. II, we describe the model Hamiltonian for the numerical calculation and the definitions of the order parameter and the correlation function. In Sec. III, we present our results for the mean occupation number distribution, the correlation function, the correlation length, the phase diagram, and the entanglement entropy obtained with a finite system. The calculations for the infinite

system are described in Sec. IV. In Sec. V, we illustrate the ground state in a different set of basis states that are categorized by the $\mathbb{Z}_2$ symmetry. Finally we conclude in Sec. VI.

II. MODEL HAMILTONIAN AND SYMMETRIES

The system we consider here is a binary BEC in a one-dimensional (1D) optical lattice with lattice constant L_0. The length scale is chosen such that $L_0 = 1$. The binary BEC consists of two hyperfine atomic states of a single species, which can be defined as spin-up and spin-down, $\sigma = \uparrow, \downarrow$. Spins of two different orientations are coupled by a two-photon transition. This can be realized in an ultracold atom gas experiment with, e.g., ^{87}Rb atoms [4].

The binary BEC in an optical lattice can be mapped to a two-component Bose-Hubbard model, which is composed of three parts,

$$\hat{H} = \hat{H}_0 + \hat{H}_I + \hat{H}_C, \tag{1}$$

where the three portions of the total Hamiltonian are given by

$$\hat{H}_0 = -J \sum_{j=1;\sigma}^{L-1} [a^\dagger_{j+1,\sigma} a_{j,\sigma} + \text{H.c.}], \tag{2}$$

$$\hat{H}_I = \frac{U}{2} \sum_{j=1;\sigma}^{L} n_{j,\sigma}(n_{j,\sigma} - 1) + U_{\uparrow\downarrow} \sum_{j=1}^{L} n_{j,\uparrow} n_{j,\downarrow}, \tag{3}$$

$$\hat{H}_C = -\Omega \sum_{j=1}^{L} (a^\dagger_{j,\uparrow} a_{j,\downarrow} + a^\dagger_{j,\downarrow} a_{j,\uparrow}), \tag{4}$$

respectively. In the above Hamiltonian, $a^\dagger_{j,\sigma}(a_{j,\sigma})$ creates (annihilates) a boson with spin orientation σ on the jth site and $n_{j,\sigma} = a^\dagger_{j,\sigma} a_{j,\sigma}$ is the corresponding occupation number operator. Bosons of either spin species can tunnel to the nearest-neighbor site with tunneling energy J, assumed here to be the same for both species. Only on-site interactions are included, with interaction energy U between same-spin species and $U_{\uparrow\downarrow}$ between different spins. The amplitude of the two-photon microwave coupling between two components is denoted as Ω. In our calculation we define the energy unit such that $J = 1$.

The interplay of the intracomponent interaction and the intercomponent interaction determines the phase of the binary BEC [5]. With no intercomponent coupling, $\Omega = 0$, and large intracomponent interaction $U > U_{\uparrow\downarrow}$, the total energy is minimized by spreading each component equally to all sites. On the other hand, whenever $U_{\uparrow\downarrow} > U$ the system phase separates [25]. This distinction can be quantified as

$$\Delta = \frac{U^2}{U^2_{\uparrow\downarrow}}, \tag{5}$$

where $\Delta > 1$ indicates a miscible phase and $\Delta < 1$ is phase separated.

Turning on the intercomponent coupling, $\Omega > 0$, the symmetry is reduced from $\text{U}(1) \times \text{U}(1)$ to $\mathbb{Z}_2 \times \text{U}(1)$ and the phase-separated state is replaced by an immiscible phase, analogous to a spin ferromagnet, where the occupation number of each component differs but the system remains translationally invariant. For sufficiently large Ω, the system is always in the miscible phase. In this paper, we consider the case $\Delta = 1/4$ and tune Ω to realize the miscible-immiscible phase transition.

In Sec. III, we consider open boundary conditions (OBCs) for a finite system of L sites and N total number of particles. Even though OBCs bring forth obstructive boundary effects, they are numerically less expensive than periodic boundary conditions. Indeed, the DMRG algorithm with periodic boundary conditions demands additional efforts for an effective simulation [26].

We focus on the phase transitions with a global filling factor $\rho = N/L = 1$. Such a system in an optical lattice can be appropriately mapped to a single-band Bose-Hubbard model [27,28].

To look into the miscible-immiscible transition we study the expectation value and the correlation function of the occupation number difference operator, which on the jth site is defined as $\Delta N_j = n_{j,\uparrow} - n_{j,\downarrow}$. Its average throughout the whole lattice,

$$M = \frac{1}{L} \sum_{j=1}^{L} \Delta N_j, \tag{6}$$

is the order parameter of the phase transition in this model. The expectation value of this order parameter is the magnetization of the system. Note that neither this order parameter nor the particle number operator for each component commutes with the total Hamiltonian (1), due to the coupling of Eq. (4).

We also study the correlation function of occupation difference operators between bosons on the jth site and the j'th site:

$$C(j, j') = \langle \Delta N_j \Delta N_{j'} \rangle. \tag{7}$$

If the system is translationally invariant, $C(j, j')$ depends only on the distance between the two sites $|j - j'|$, and thus we can define $C(j) = C(0, j)$.

It is important to consider the symmetries of the model. First, the Hamiltonian has U(1) symmetry as it commutes with the total number operator N. Second, the Hamiltonian has a discrete $\mathbb{Z}_2$ symmetry as the Hamiltonian is unchanged if all the spins are flipped. We show in the following sections that this symmetry is spontaneously broken when Ω is below the critical value.

III. FINITE SYSTEM RESULTS

In this paper we consider the phase transition occurring in the Mott insulator (MI) regime. Actually the critical point separating the superfluid (SF) and the MI regime has not been documented in the literature for a linearly coupled two-component BEC in optical lattices [29]. In the MI regime the energy scale of the system is dominated by the on-site interaction energy. The coexistence of multiple bosons on the same lattice site is energetically expensive for integer filling and thus particles are equally spread over all lattice sites. The local particle number fluctuation vanishes in the ground state. The excited state is gapped from the ground state in the MI regime and contains pairs of quasiparticles and quasiholes.

MPSs are an excellent ansatz for the ground state of a gapped system. A mean-field derivation can approximate this system in the SF regime and predicts the critical value for Ω as [11,12]

$$\Omega_c = U\rho\left(\frac{1}{\sqrt{\Delta}} - 1\right). \tag{8}$$

Below we show that MPSs provide a more accurate MI ground state than the mean-field theory and predict a different power-law dependence of Ω_c on U that agrees with a second-order perturbation theory.

A basic question is still open: where is the border between the SF regime and the MI regime for this linearly coupled two-component Bose-Hubbard model? For this two-component model, the additional degrees of freedom give rise to two branches of the quasiparticle spectrum [30]. In the absence of the coupling Ω between the two components the two branches are independent. When the coupling is turned on, one branch accounts for the SF-MI transition but the other depends on Ω and is responsible for the miscible-immiscible phase transition, which is addressed in Sec. V.

The border can be determined by locating the value of on-site interaction where the energy gap closes. The energy gap can be simply verified numerically by calculating the ground-state energy E for systems of $N-1$, N, and $N+1$ total particles. The system has integer filling factor when the total number of particles is N. The energy gap ΔE can be obtained by the formula

$$\Delta E = E(N+1) + E(N-1) - 2E(N). \tag{9}$$

Within numerical accuracy, the simulation gives $\Delta E \neq 0$ for a system with parameters in the MI regime. This will be addressed in a subsequent publication [31].

In the following finite DMRG calculations, we choose the number of states $m = 300$ for the MPS, which is large enough to ensure the variational ground state is close to the true ground state, while being computationally efficient.

A. Occupation distribution

We first show the immiscible and miscible phases by displaying the occupation distribution throughout a lattice. In Fig. 1, we plot the mean occupation number for (a) $\Omega \ll \Omega_c$, (b) $\Omega \lesssim \Omega_c$, and (c) $\Omega \gg \Omega_c$.

When $\Omega \ll \Omega_c$, the system is in the immiscible phase, where the largest energy scale in the system is the intercomponent interaction strength. The coexistence of different boson species costs more energy compared to the same species; therefore states with only one component on each site are favorable. We recall the total Hamiltonian (1) preserves the $\mathbb{Z}_2$ symmetry, as the energy is unchanged when all spin orientations are flipped. In the thermodynamic limit, the ground state is twofold degenerate. The $\mathbb{Z}_2$ spontaneous symmetry breaking will occur in this regime of Ω. On the other hand, in principle, for a finite-size system spontaneous symmetry breaking should not occur. Nevertheless, obviously in Fig. 1(a) the ground state in the immiscible phase does not preserve the $\mathbb{Z}_2$ symmetry of the total Hamiltonian with the imbalance $\langle \Delta N \rangle \neq 0$ in mean occupation numbers for two components.

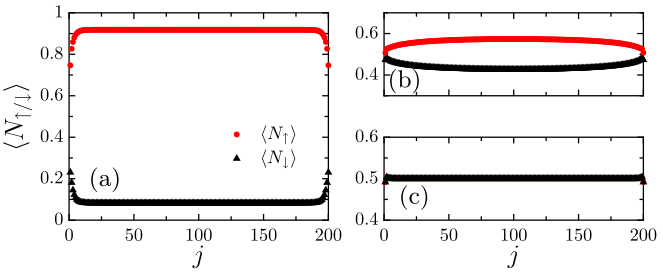

FIG. 1. (Color online) Mean occupation number for spin-up bosons $\langle N_\uparrow \rangle$ (red circles) and spin-down bosons $\langle N_\downarrow \rangle$ (black triangles) on the jth site throughout a 200-site lattice with an open boundary condition (a) below, (b) near but still below, and (c) above the critical point in the MI regime. The interaction strengths are $U = 5$ and $U_{\uparrow\downarrow} = 2U$. The linear coupling strengths are (a) $\Omega = 0.18$, (b) $\Omega = 0.214$, and (c) $\Omega = 0.248$.

In the ground-state subspace, the DMRG variational calculation adopts the lowest-entropy state and therefore numerically enforces the order of the symmetry breaking state. In a numerical DMRG calculation the broken symmetry state is variationally favored if the energy splitting of the ground state is smaller than the energy scale set by the truncation error of the calculation. There is randomness in this favoredness. In a real-life numerical simulation many factors, e.g., the direction of the DMRG variational algorithm, may determine which component will appear in the favorable states. In order to show the randomness, for each value of Ω we start the DMRG simulation with a different random initial wave function. The probability that one of the two components is preferred by random fluctuation is one half. Consequently, when the system is in the immiscible phase we saw the domination of spin-up bosons in half of the simulations and the domination of spin-down bosons in the other half (not shown here).

As the coupling coefficient Ω increases, the imbalance in occupation decreases, reaching zero at the critical point as can be seen in Fig. 1(b). Above the critical point, the ground state has the same $\mathbb{Z}_2$ symmetry of the Hamiltonian and both components equally occupy all of the sites. Therefore the imbalance must be zero and the system is in the miscible phase [see Fig. 1(c)].

One must always be aware of the boundary effects when we approximate a system in the thermodynamic limit with a finite system. The boundary effect comes from the correlation between a particle in the bulk of the finite system and a particle on the boundary, where particles can hop only in one direction. As we can see in Fig. 1(a), near the boundary the mean occupation number for both spin-up and spin-down bosons deviates from the bulk. It decreases the mean occupation number of the dominant component and increases that of the other component. Approaching the critical point, the correlation between two sites at longer distance starts to become non-negligible, as we expect for a second-order phase transition. Consequently the boundary effect more strongly influences the sites in the bulk of the lattice, as can be seen in Fig. 1(b). When the coupling coefficient is sufficiently close to the critical point, the influence of both boundaries merge together and we see two curved lines for the mean occupation number of both components. The boundary effect

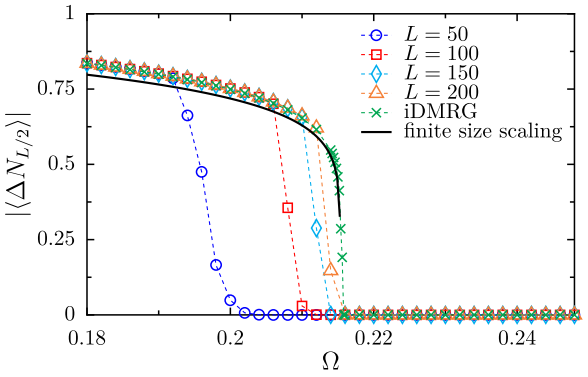

FIG. 2. (Color online) The absolute occupation imbalance $|\langle \Delta N \rangle|$ on the middle site $L/2$ of lattices having 50 (blue circles), 100 (red squares), 150 (cyan diamonds), and 200 (orange triangles) sites as a function of the coupling coefficient Ω, when $U = 5$ and $U_{\uparrow\downarrow} = 2U$. The green crosses are the data for an infinite lattice from iDMRG calculations. The dashed lines are used to guide the eyes. The solid black line is drawn with parameters from a finite-size scaling about the critical point with exponent $\beta = 1/8$.

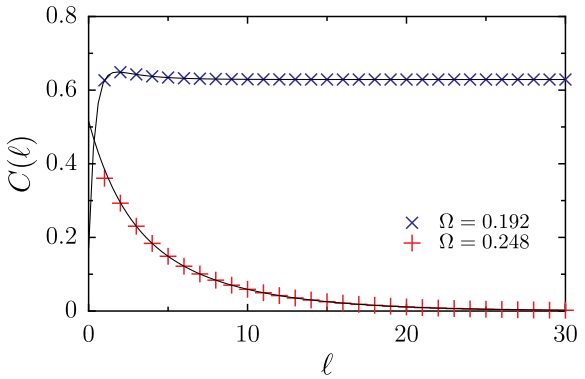

FIG. 3. (Color online) The correlation function $C(\ell)$ calculated in the bulk of a lattice with 200 sites with 60 sites cut off at both ends. The blue crosses (red pluses) are the values of the correlation function between the zeroth site and the ℓth site when $\Omega = 0.192$ ($\Omega = 0.248$), which is below (above) the critical point. The curves are the fittings with respect to a sum of two exponential functions. The interaction strengths are $U = 5$ and $U_{\uparrow\downarrow} = 2U$.

is negligible above the critical point [see Fig. 1(c)]. The effect of the boundaries on the calculation of the correlation function is explored in more detail in the following subsection.

In Fig. 2, we show the absolute imbalance $\langle \Delta N_{L/2} \rangle$ as a function of the coupling coefficient Ω for different lattice sizes. As we have discussed above, below the critical value Ω_c the imbalance is nonzero and drops quickly to zero at the critical point. We can see that Ω_c clearly saturates as the system size is increased towards the thermodynamic limit. From Fig. 2, the critical point can be estimated as $\Omega_c \approx 0.215$. We improve on this estimate in Sec. III C below.

By using finite-size scaling, we can extract the critical coupling Ω_c and critical exponents by collapsing curves for lattices of different lengths [32]. First we define the reduced coupling $\epsilon = |1 - \Omega/\Omega_c|$. Previous studies in the literature have indicated this phase transition is of second order [15]. Near the critical point of a second-order phase transition, we know that the correlation length and magnetization satisfy $\xi \propto \epsilon^{-\nu}$ and $M \propto \epsilon^{\beta}$, respectively (only below the critical point, otherwise $M = 0$), from which we can deduce the relation $M \propto \xi^{-\beta/\nu}$. For a finite lattice, instead of approaching zero when ξ diverges, M stays at a finite nonzero value when ξ becomes comparable to the lattice length L. This behavior can be described by $M = \xi^{-\beta/\nu} M_0(L/\xi)$ with the assisting function $M_0(x)$ that goes to zero as $x^{-\beta/\nu}$ when $x \to 0$ and is a constant when $x \to \infty$. To remove the size dependence, we define the scaling function

$$\tilde{M}(L^{1/\nu}\epsilon) = L^{\beta/\nu} M(\epsilon). \tag{10}$$

With $\nu = 1$ and $\Omega_c = 0.2153$ that we obtain in the next subsections, we find that the four curves from Fig. 2 coalesce with $\beta = 1/8$ (not shown here). In Fig. 2, we plot the curve ϵ^{β} with $\beta = 1/8$ obtained from the finite-size scaling and $\Omega_c = 0.2153$. We find that near the critical point it agrees very well with the results from the iDMRG calculations in Sec. IV.

B. Correlation function and correlation length

Close to the boundary the quantum state may deviate dramatically from the infinite system due to the inevitable boundary effect (see Fig. 1). For this reason, in order to simulate the correlation in the thermodynamic limit with a finite-size system, we investigate only the correlation function computed in the bulk of the lattice, where the boundary effect is minimized. Keeping this in mind is particularly important when $\Omega < \Omega_c$ [see Fig. 1(a)]. Very close to the critical point the boundary effects cannot be neglected. In this region the correlation function is not reliable for extracting the correlation length. For instance, to calculate the two-point correlator (7) in Fig. 3 for a lattice of 200 sites, we cut off 60 sites at both ends of the lattice. In Fig. 3 we show the correlation function up to 30 sites. The correlation function depends only on the distance $|j - j'|$ between its two studied sites. Consequently we enumerate only the distance by $\ell = |j - j'|$. For $\Omega = 0.192 \ll \Omega_c$, in Fig. 3, we find at short distances the correlation function first increases and then decreases exponentially before saturating at a nonzero value. The short range behavior most likely stems from the finite-size effects, since in iDMRG calculations the correlation function decreases only exponentially and saturates to a nonzero value. For $\Omega = 0.248 \gg \Omega_c$ in the miscible phase, the correlation function exponentially decays to zero.

As suggested by the characteristic form of correlation functions in the MPS [23,33] and the fact that the correlation length decays exponentially in a system away from criticality, the correlation function can be fitted with a sum of exponential functions. Here we fit the correlation function with a sum of two exponential functions:

$$C(\ell) = \sum_{i=1,2} a_i \exp(-\ell/\xi_i) + c, \tag{11}$$

where the constant c has a nonzero value when Ω is below the critical point. We find in Fig. 3 that the fitting precisely captures the behavior of the correlation function.

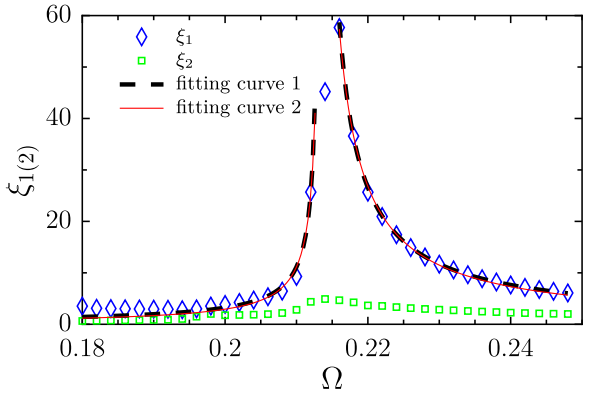

FIG. 4. (Color online) The longer (blue diamonds) and shorter (green squares) correlation lengths extracted by fitting the correlation function with a sum of two exponential functions for a lattice of 200 sites. The longer correlation length shows divergence in a certain region of the coupling coefficient Ω. The black dashed line shows the fitting curve with the critical exponent ν as an independent variable and the red solid line shows the fitting curve with the plausible fixed exponent $\nu = 1$ (see text). The interaction strengths are $U = 5$ and $U_{\uparrow\downarrow} = 2U$.

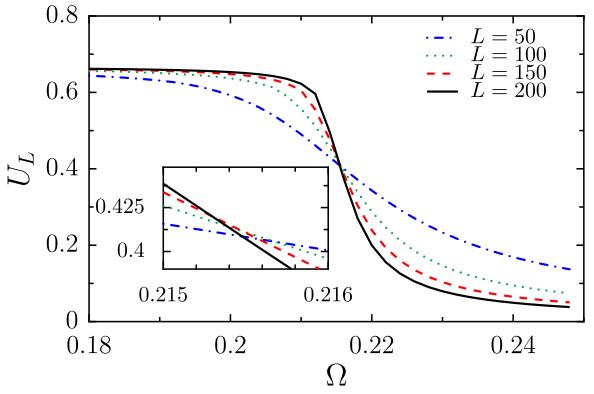

FIG. 5. (Color online) The Binder cumulant U_L, Eq. (12), as a function of the coupling coefficient Ω for lattices of $L = 50$ (blue dash-dotted curve), 100 (green dotted curve), 150 (red dashed curve), and 200 (black solid curve), when $U = 5$ and $U_{\uparrow\downarrow} = 2U$. The inset zooms into the region where four curves cross each other, near $\Omega_c = 0.2153$.

In Fig. 4, we plot the two correlation lengths from the fitting function (11). The longer correlation length ξ_1 shows clear divergent behavior around $\Omega = 0.215$, which characterizes the behavior of the system close to criticality. In principle, the shorter correlation length ξ_2 will also diverge at the critical point [21], but this is difficult to determine from finite-size simulations because the correlation length is much shorter than ξ_1. We fit the correlation length with the power law $\xi_1 \propto |\Omega - \Omega_c|^{-\nu}$ around the critical point. In the first fitting, shown in Fig. 4, we set ν as an independent variable and obtain the following optimized fitting function:

$$\xi_1(\Omega) = \begin{cases} \frac{0.07144\pm0.0342}{|0.2133\pm0.0001-\Omega|^{0.8844\pm0.0336}}, & \Omega < \Omega_c, \\ \frac{0.2797\pm0.0369}{|0.2131\pm0.0002-\Omega|^{0.915\pm0.0336}}, & \Omega > \Omega_c. \end{cases}$$

On account of the nonlinear least-square algorithm's numerical complexity, combined with the less reliable data near the critical point, the exponent ν may have low numerical accuracy. Nevertheless, they are close to the already known value $\nu = 1$ in the conformal field theory (CFT) for the 1D quantum Ising model with a transverse magnetic field. Therefore for a second fitting, also shown in Fig. 4, we set $\nu = 1$ and obtain

$$\xi_1(\Omega) = \begin{cases} \frac{0.04014\pm0.00825}{|0.2135\pm0.0004-\Omega|}, & \Omega < \Omega_c, \\ \frac{0.2014\pm0.005}{|0.2125\pm0.0001-\Omega|}, & \Omega > \Omega_c. \end{cases}$$

The closeness of these two fit functions in Fig. 4 shows the difficulty in obtaining accurate values of ν and Ω_c by this method. The critical point $\Omega_c = 0.213$ is somewhat below the result obtained from Fig. 2 ($\Omega_c = 0.2153$) and demonstrates the accuracy of this fitting technique. The fitting for the parameter above the critical point is better than the other side in the coupling coefficient space. The reason is due to the less severe boundary effect above the critical point. It can be seen in Fig. 4 that both curves fit the data points very well, with only slight deviations when the coupling coefficient is far away from the critical point. In any event, this suggests that $\nu = 1$ is likely, as consistent with already known theories.

C. Binder cumulant

The Binder cumulant can be used to more accurately determine the critical point in the thermodynamic limit from finite-size calculations [34,35]. Its potential usefulness and generalizations still attract a lot of attention [36,37]. With the Binder cumulant the critical point can be determined with a relatively small finite-size lattice. For example, the critical temperature for a two-dimensional Ising model can be obtained from the Binder cumulant with a 9×9 lattice [34].

The Binder cumulant for this system U_L is defined as

$$U_L = 1 - \frac{\langle M^4 \rangle}{3\langle M^2 \rangle^2}, \tag{12}$$

where $\langle M^2 \rangle$ and $\langle M^4 \rangle$ are the second-order and the fourth-order moments of the order parameter, respectively. Note that the Binder cumulant depends on the length L of the lattice.

In Fig. 5, we plot the Binder cumulant with the same parameters and the same OBCs we have used for the preceding subsections for lattices of a variety of lengths. The curves clearly show the asymptotic behavior of the Binder cumulant: It decreases with increasing Ω and asymptotically approaches 2/3 and 0 below and above the critical point, respectively. Near the critical point, it decreases faster than in other regions. In addition, the data for a larger lattice exhibit a steeper transition near Ω_c. As a result, the different curves cross each other at the critical point. In the thermodynamic limit the curve should be discontinuous at the critical point.

As we can see in Fig. 5, the four curves cross in a small range of Ω. The inset of Fig. 5 shows the crossing is located in the region [0.2152 0.2158]. The value of Ω for the crossing point corresponds to the critical value Ω_c. The cubic spline interpolation of the curves for $L = 150$ and 200 suggests the critical point should be at $\Omega_c = 0.2153$. In Sec. III A, we performed the finite-size scaling with this value as the tentative critical value and obtained the expected value for the exponent

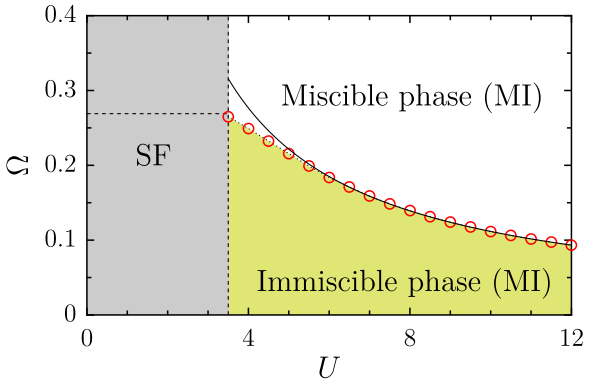

FIG. 6. (Color online) The phase diagram in the space of the coupling parameter Ω and the on-site intracomponent interaction U. The intercomponent interaction $U_{\uparrow\downarrow} = 2U$. The border between the superfluid and the MI will be updated in upcoming works. The red circles are the data points of the border between miscible and immiscible phases determined by the Binder cumulant for lattices of $L = 50$ and $L = 100$. The dotted curve connecting the red circles interpolates the data points (red circles). The solid curve is attained by fitting the data points with C/U for $U > 10$.

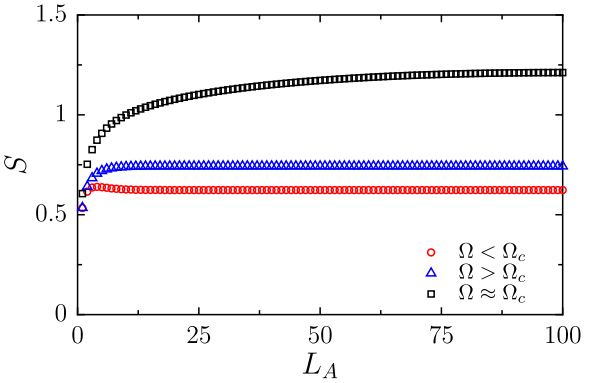

FIG. 7. (Color online) The entanglement entropies up to half of a 200-site lattice, below (red circles), near (blue triangles), and above (black squares) the critical point in the MI regime. The interaction strengths are $U = 5$ and $U_{\uparrow\downarrow} = 2U$.

β. In the following section we see this value also agrees with the iDMRG results.

D. Phase diagram

As seen in the last subsection, the Binder cumulant can locate the critical point very precisely. Using this measure, in Fig. 6, we now plot the phase diagram of this model Hamiltonian in the space of Ω and U, while keeping $U_{\uparrow\downarrow} = 2U$, corresponding to $\Delta = 1/4$. In Fig. 5, we see that increasing the number of lattice sites changes only the value of Ω_c in the fourth digit after the decimal point. As a consequence, to speed the calculation, we locate Ω_c by using Binder cumulants for shorter lattices of $L = 50$ and $L = 100$.

In Fig. 6 for the MI regime, we see the critical value Ω_c decreases as U is increased as approximately $1/U$. This result is in contrast to mean-field predictions, which show linear dependence of Ω_c on U [12].

When U and $U_{\uparrow\downarrow}$ are large, the tunneling between sites is negligible. Perturbation theory can be employed in the parameter J to find a further approximation to provide more insight into the underlying physics. Using the strong-coupling expansion, we derived the effective Hamiltonian for this model, which turns out to be a ferromagnetic *XXZ* model with a transverse magnetic field:

$$H = -J_\perp \sum_j \left[S_j^x S_{j+1}^x + S_j^y S_{j+1}^y\right] + J_z \sum_j S_j^z S_{j+1}^z + \Gamma \sum_j S_j^x, \quad (13)$$

where S_j^x, S_j^y, and S_j^z are the three components of the spin-operator for a spin-1/2 particle on the jth lattice site, respectively.

The coefficients for the effective Hamiltonian are

$$J_\perp = \frac{4}{U_{\uparrow\downarrow}}, \quad J_z = \frac{4}{U_{\uparrow\downarrow}} - \frac{8}{U}, \quad \Gamma = -2\Omega. \quad (14)$$

For the parameters we have chosen $U_{\uparrow\downarrow} = 2U$, viz., $|J_z/J_\perp| = 3$, which indicates the ferromagnetic ground state when $\Omega = 0$. When $|J_z/J_\perp| \to \infty$, i.e., the first term in Eq. (13) can be neglected, this model can be further mapped onto the Ising model in a transverse magnetic field, for which we know the phase transition occurs at $\Gamma_c = J_z/2$. For nonzero but small $J_\perp$, the exact dependence of Γ_c on $J_\perp$ and J_z is not known, but we expect that $\Gamma_c \propto 1/U$.

In Fig. 6, in the region where $U > 10$ we fit the data points on the border line between the miscible and the immiscible phase to the function C/U and find the coefficient $C \approx 1.09$, in excellent agreement with what we obtained from the DMRG calculation for the *XXZ* model with a transverse field, where we found $\Gamma_c = 0.36 J_z$. Since $J_z = -6/U$, we obtain $\Gamma_c = 2.16/U$ and $\Omega_c = 1.08/U$.

E. Entanglement entropy

It has been demonstrated that the entanglement entropy, which is a significant concept in quantum information, also plays an important role in understanding quantum phase transitions in condensed matter physics since it is related to the appearance of long-range correlations [38,39]. The bipartite entanglement entropy can capture the large-scale behavior of quantum correlations in the critical regime. In the vicinity of the critical point Ω_c, the entanglement entropy diverges logarithmically with the correlation length. Here we present the scaling behavior of entanglement entropy for the model and determine the central charge at criticality.

Suppose the lattice is divided into sublattice A on the left and sublattice B on the right. We define the entanglement entropy as the von Neumann entropy of either one of the two sublattices, say sublattice A,

$$S = -\mathrm{Tr}[\rho_A \log(\rho_A)], \quad (15)$$

where $\rho_A = \mathrm{Tr}_B(\rho)$ is the reduced density matrix for part A.

In Fig. 7, we plot the entanglement entropy for $\Omega < \Omega_c$, $\Omega \approx \Omega_c$, and $\Omega > \Omega_c$ as the size of sublattice A is increased

up to the half of the whole lattice. We find the bipartite entanglement entropy increases as the block size increases. When it is off-critical, entanglement entropy saturates above some critical length which is proportional to the correlation length ξ as determined in Sec. III B.

In Ref. [39], the critical entanglement entropy is shown to coincide with the entropy in the CFT for a variety of spin chains. Consequently, the central charge can be extracted from the critical entanglement entropy. As derived in Ref. [40], the critical entanglement entropy satisfies

$$S \approx \frac{c+\bar{c}}{6} \log\left[\frac{2L}{\pi} \sin\left(\frac{\pi L_A}{L}\right)\right] + k, \qquad (16)$$

for a finite lattice of total size L and a sublattice of size L_A with periodic boundary conditions, where c and $\bar{c}$ are holomorphic and antiholomorphic central charges of the CFT and k is a model-dependent constant. For OBCs, only the holomorphic central charge is expected.

We should point out the model-dependent constant k here is generally nonzero, unlike other widely studied models. For instance, in the quantum Ising model, the ordered state with zero transverse field is a product state. The entanglement entropy of such a totally ordered state is zero and therefore $k = 0$. On the other hand, for the two-component Bose-Hubbard model the entanglement entropy away from the critical point approaches that of the gapped MI system when $\Omega \to 0$. This is vanishing only when $(U, U_{\uparrow\downarrow}) \to \infty$; otherwise the remaining local particle number fluctuation contributes to the entanglement entropy as a correction to the CFT prediction.

In extracting the central charge, there are numerical difficulties due to the OBCs. For this reason, we use periodic boundary conditions. For the *XXZ* Hamiltonian (13), from our numerical calculation we confirmed the central charge $c = 1/2$, corresponding to the universality class of the transverse-field Ising model. For the Hamiltonian (1) with periodic boundary conditions, we also successfully extracted the central charge $c = 1/2$ when $U \to \infty$, consistent with the critical exponents we obtained above.

IV. SIMULATIONS WITH iDMRG

So far we have simulated a system only for a finite-size lattice. The expectation values of the physical quantities are therefore somewhat affected by finite-size effects and the boundary effects that break the translational invariance of a system. To remove these drawbacks, we now use the iDMRG [24], which is a better ansatz for a translational invariant system.

In Fig. 2, the green crosses show the mean occupation number imbalance obtained from iDMRG calculations. We can see it matches very closely the asymptotic result of the finite DMRG calculation at the critical point.

Due to the translational invariance, the MPS is represented by a repeated unit cell consisting of a single site. While the correlation length can be extracted from the correlation function, it can also be directly calculated from the spectrum of the transfer matrix, which originates from the exponentially decaying nature of MPS correlations [23,33].

The correlation length obtained in this fashion increases as the number of states m (dimension of the MPS representation) is increased. For a gapped noncritical system, it saturates at a certain value of m, while for a gapless critical system it diverges with m, and this is demonstrated in Fig. 8. Up to $m = 300$, all the curves exhibit saturation behavior except the curve for $\Omega = 0.2154$. Therefore, the critical point is close to $\Omega = 0.2154$, which agrees quite well with the value $\Omega_c = 0.2153$ from the Binder cumulant for finite systems.

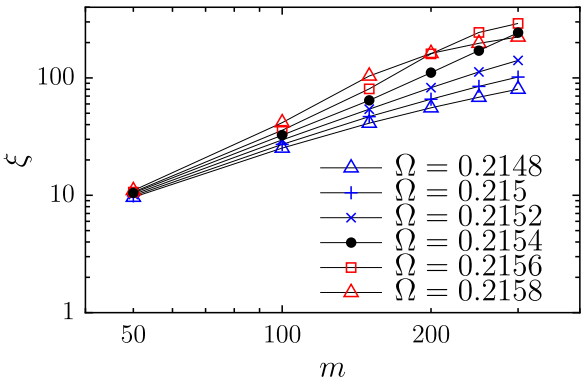

FIG. 8. (Color online) Correlation length vs number of states for various values of the coupling coefficient Ω around the critical point in the MI regime. The other parameters are $U = 5$ and $U_{\uparrow\downarrow} = 2U$.

In Fig. 9, we plot the correlation length as a function of Ω for $m = 50$ and 300. When $m = 50$, the correlation length is larger near the critical point but the divergent behavior is not obvious. However, it is clear for $m = 300$. We also plot the correlation length when m is extrapolated to infinity in Fig. 9. The error bars show the uncertainty increases as Ω is closer to Ω_c. Combining these uncertainties, we find that a fit of this curve with $\xi \propto |\Omega - \Omega_c|^{-\nu}$ gives $\nu = 0.8979 \pm 0.3857$ when $\Omega < \Omega_c$ and $\nu = 0.9621 \pm 0.0732$ when $\Omega > \Omega_c$, which is close to the known value $\nu = 1$ for the CFT for the 1D quantum Ising model with a transverse magnetic field, and a better approximation than the fitted correlation length for finite-size calculations presented in Sec. III B above.

Although the correlation lengths obtained in this section differ from those in Sec. III B (compare Figs. 4 and 8), its

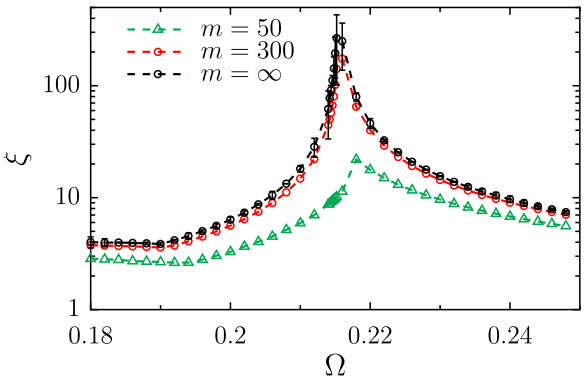

FIG. 9. (Color online) The correlation length obtained from iDMRG calculations for a translationally invariant infinite lattice with the increasing size of the number of states: $m = 50$ (green triangles), $m = 300$ (red circles), and $m = \infty$ (black circles). The data for $m = \infty$ are obtained by extrapolation. The error bars show the uncertainty in the extrapolation. The other parameters are $U = 5$ and $U_{\uparrow\downarrow} = 2U$.

characteristic divergent behavior at the criticality can be identified with both methods. The difference in the correlation length and the exponent mainly stems from finite-size effects and boundary effects in finite lattices, as discussed in Secs. III A and III B.

V. $U(1)$-$\mathbb{Z}_2$ SYMMETRY

The total Hamiltonian (1) satisfies $\mathbb{Z}_2$ symmetry because it remains unchanged if all spins are flipped. The ground state should preserve the same $\mathbb{Z}_2$ symmetry to be symmetric or antisymmetric, although computationally this is not the case for the symmetry breaking state when $\Omega < \Omega_c$. However, we can always unitarily transform the Hilbert space composed of product Fock states into one composed of symmetric and antisymmetric basis states. The new Hilbert space can provide us with further insights into how the $\mathbb{Z}_2$ symmetry is broken and restored across the critical point.

The unitary transformation for a single lattice site is

$$b_s = \frac{1}{\sqrt{2}}(a_\uparrow + a_\downarrow), \tag{17}$$

$$b_a = \frac{1}{\sqrt{2}}(a_\uparrow - a_\downarrow). \tag{18}$$

The inverse relation can be obtained by simple linear combinations:

$$a_\uparrow = \frac{1}{\sqrt{2}}(b_s + b_a), \tag{19}$$

$$a_\downarrow = \frac{1}{\sqrt{2}}(b_s - b_a). \tag{20}$$

The choice of coefficient $1/\sqrt{2}$ preserves the commutation relation:

$$[b_{s(a)}, b^\dagger_{s(a)}] = 1. \tag{21}$$

Substituting Eqs. (19) and (20) into the three portions of the total Hamiltonian (1), we have the Hamiltonian in terms of $(b^\dagger_{s(a)}, b_{s(a)})$ operators.

First the noninteracting part, Eq. (2),

$$\hat{H}_0 = -J \sum_{j=1}^{L-1} \sum_{p=s,a} [b^\dagger_{j+1,p} b_{j,p} + \text{H.c.}]. \tag{22}$$

As no spin-flipping exists in the original Hamiltonian (2), symmetry is conserved during the tunneling.

The on-site interaction Hamiltonian, the first term of Eq. (3), between the particles of the same component transforms to

$$\hat{H}_U = \frac{U}{4} \sum_{j=1}^{L} \sum_{p=s,a} N_{j,p}(N_{j,p} - 1) + \frac{U}{4} \sum_{j=1}^{L} (b^\dagger_{j,s} b^\dagger_{j,s} b_{j,a} b_{j,a} + b^\dagger_{j,a} b^\dagger_{j,a} b_{j,s} b_{j,s}) + U \sum_{j=1}^{L} N_{j,s} N_{j,a}, \tag{23}$$

where $N_{j,p} = b^\dagger_{j,p} b_{j,p}$ is the number operator for the symmetric state $(p = s)$ or the antisymmetric state $(p = a)$. The Hamiltonian describing the interaction between the two components, the second term of Eq. (3), becomes

$$\hat{H}_{U_{\uparrow\downarrow}} = \frac{U_{\uparrow\downarrow}}{4} \sum_{j=1}^{L} [N_{j,s}(N_{j,s} - 1) + N_{j,a}(N_{j,a} - 1) - (b^\dagger_{j,s} b^\dagger_{j,s} b_{j,a} b_{j,a} + b^\dagger_{j,a} b^\dagger_{j,a} b_{j,s} b_{j,s})]. \tag{24}$$

The two interaction Hamiltonians, Eqs. (23) and (24), contain terms that annihilate pairs of symmetric bosons and create pairs of antisymmetric bosons, and vice versa, but with opposite signs.

The linear coupling Hamiltonian, Eq. (4), between two components becomes

$$\hat{H}_C = -\Omega \sum_{j=1}^{L} (N_{j,s} - N_{j,a}). \tag{25}$$

This term effectively has the function of an unbalanced chemical potential, favoring particles in the symmetric state as Ω is increased.

We also employ the iDMRG algorithm to obtain the optimized infinite MPS with the Hamiltonian given above. In Fig. 10, we plot the mean occupation number for symmetric and antisymmetric states. As expected from the analysis of the linear coupling Hamiltonian, more and more bosons occupy the symmetric states with increasing Ω. There is a kink around the critical point Ω_c. To see this kink more closely, we also plot the derivative of the curve. At the critical point, the derivative diverges.

We find that the derivatives of the mean occupation number for both symmetric and antisymmetric states can be fitted with $K \log \Omega$, as shown by the solid curves in Fig. 10. This is further numerical evidence that the linearly coupled two-component Bose-Hubbard model we are studying is equivalent to a 1D quantum Ising model with a transverse magnetic field, which gives a logarithmic divergence with the critical exponent $\alpha = 0$ [21].

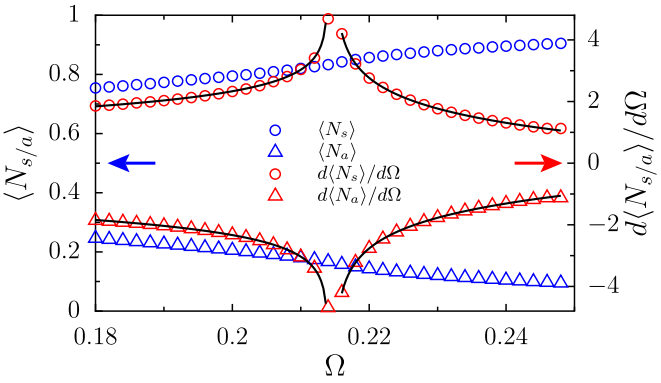

FIG. 10. (Color online) The mean occupation number and its derivative with respect to Ω for symmetric states and antisymmetric states around the critical point when $U = 5$ and $U_{\uparrow\downarrow} = 2U$. The black solid curves are the fitting curves for the derivatives to a logarithmic function. The arrows point to the corresponding y axis of the mean occupation number or its derivative.

VI. CONCLUSION

In this paper we have comprehensively studied the miscible-immiscible phase transition in a linearly coupled two-component Bose-Hubbard model. We focus on this model in the MI regime with a filling factor of 1, i.e., the total number of particles is equal to the number of lattice sites. We simulate this system by using both finite DMRG and iDMRG algorithms.

We have illustrated the basic features of this phase transition. Below the critical point $\Omega < \Omega_c$ the computations giving symmetry broken states show an imbalanced mean occupation number. The imbalance decreases and disappears at the critical point. Above the critical point the imbalance is zero and the $\mathbb{Z}_2$ symmetry of flipping the spins is restored in the ground state. The correlation functions of the occupation imbalance operator show exponential decay when it is off-critical. The extracted correlation length diverges with a power-law exponent ν close to 1, and critical exponents $\alpha = 0$ and $\beta = 1/8$.

We employed the Binder cumulant to determine the critical value of the linear tunneling coefficient and determined the phase diagram. A strong-coupling expansion reveals that in the MI regime this model is equivalent to a *XXZ* model with a transverse magnetic field.

The phase transition is also characterized by the entanglement entropy, which diverges logarithmically at the critical point and otherwise saturates. The central charge at the critical point was extracted from DMRG calculations with periodic boundary conditions. All of these results demonstrate conclusively that the transition is in the universality class of the $c = 1/2$ CFT.

Note added. Recently, we became aware of other authors studying the same model [41].

ACKNOWLEDGMENTS

We acknowledge support from the Australian Research Council Centre of Excellence for Engineered Quantum Systems and the Discovery Projects funding scheme (Projects No. DP1092513 and No. DP110101047).

[1] M. Greiner, O. Mandel, T. Esslinger, T. W. Hänsch, and I. Bloch, Nature (London) **415**, 39 (2002).
[2] I. Bloch, J. Dalibard, and S. Nascimbène, Nat. Phys. **8**, 267 (2012).
[3] J. Stenger, S. Inouye, D. M. Stamper-Kurn, H.-J. Miesner, A. P. Chikkatur, and W. Ketterle, Nature (London) **396**, 345 (1998).
[4] D. S. Hall, M. R. Matthews, J. R. Ensher, C. E. Wieman, and E. A. Cornell, Phys. Rev. Lett. **81**, 1539 (1998).
[5] T.-L. Ho and V. B. Shenoy, Phys. Rev. Lett. **77**, 3276 (1996).
[6] H. Pu and N. P. Bigelow, Phys. Rev. Lett. **80**, 1130 (1998).
[7] E. Timmermans, Phys. Rev. Lett. **81**, 5718 (1998).
[8] B. Paredes and J. I. Cirac, Phys. Rev. Lett. **90**, 150402 (2003).
[9] A. Kuklov, N. Prokof'ev, and B. Svistunov, Phys. Rev. Lett. **92**, 030403 (2004).
[10] O. E. Alon, A. I. Streltsov, and L. S. Cederbaum, Phys. Rev. Lett. **97**, 230403 (2006).
[11] J. Sabbatini, W. H. Zurek, and M. J. Davis, Phys. Rev. Lett. **107**, 230402 (2011).
[12] J. Sabbatini, W. H. Zurek, and M. J. Davis, New J. Phys. **14**, 095030 (2012).
[13] J. M. Zhang, C. Shen, and W. M. Liu, Phys. Rev. A **85**, 013637 (2012).
[14] E. Altman, W. Hofstetter, E. Demler, and M. D. Lukin, New J. Phys. **5**, 113 (2003).
[15] I. M. Merhasin, B. A. Malomed, and R. Driben, J. Phys. B: At. Mol. Opt. Phys. **38**, 877 (2005).
[16] J. Williams, R. Walser, J. Cooper, E. Cornell, and M. Holland, Phys. Rev. A **59**, R31 (1999).
[17] Q.-H. Park and J. H. Eberly, Phys. Rev. A **70**, 021602 (2004).
[18] C. Lee, Phys. Rev. Lett. **102**, 070401 (2009).
[19] E. Nicklas, H. Strobel, T. Zibold, C. Gross, B. A. Malomed, P. G. Kevrekidis, and M. K. Oberthaler, Phys. Rev. Lett. **107**, 193001 (2011).
[20] S. De, D. L. Campbell, R. M. Price, A. Putra, B. M. Anderson, and I. B. Spielman, Phys. Rev. A **89**, 033631 (2014).
[21] J. Cardy, *Scaling and Renormalization in Statistical Physics*, Cambridge Lecture Notes in Physics (Cambridge University Press, Cambridge, UK, 1996).
[22] D. Schrader, I. Dotsenko, M. Khudaverdyan, Y. Miroshnychenko, A. Rauschenbeutel, and D. Meschede, Phys. Rev. Lett. **93**, 150501 (2004)
[23] U. Schollwöck, Ann. Phys. **326**, 96 (2011).
[24] I. P. McCulloch, arXiv:0804.2509.
[25] F. Zhan and I. P. McCulloch, Phys. Rev. A **89**, 057601 (2014).
[26] P. Pippan, S. R. White, and H. G. Evertz, Phys. Rev. B **81**, 081103 (2010).
[27] D. van Oosten, P. van der Straten, and H. T. C. Stoof, Phys. Rev. A **67**, 033606 (2003).
[28] M. Greiner, I. Bloch, O. Mandel, T. W. Hänsch, and T. Esslinger, Phys. Rev. Lett. **87**, 160405 (2001).
[29] But see some indications from the phase diagram in Fig. 1 of Ref. [41].
[30] P. Tommasini, E. J. V. de Passos, A. F. R. de Toledo Piza, M. S. Hussein, and E. Timmermans, Phys. Rev. A **67**, 023606 (2003).
[31] F. Zhan, J. Sabbatini, M. J. Davis, and I. P. McCulloch (unpublished).
[32] M. N. Barber, in *Phase Transition and Critical Phenomena* (Academic, London, 1983), Vol. 8, pp. 146–259.
[33] S. Östlund and S. Rommer, Phys. Rev. Lett. **75**, 3537 (1995).
[34] K. Binder, Phys. Rev. Lett. **47**, 693 (1981).
[35] B. Kastening, Phys. Rev. E **87**, 044101 (2013).
[36] M. Hasenbush, J. Stat. Mech. (2008) P08003.
[37] W. Selke and L. N. Shchur, Phys. Rev. E **80**, 042104 (2009).
[38] T. J. Osborne and M. A. Nielsen, Phys. Rev. A **66**, 032110 (2002).
[39] G. Vidal, J. I. Latorre, E. Rico, and A. Kitaev, Phys. Rev. Lett. **90**, 227902 (2003).
[40] P. Calabrese and J. Cardy, J. Stat. Phys. (2004) P06002.
[41] L. Barbiero, M. Abad, and A. Recati, arXiv:1403.4185.